

Effect of melt height and obstacle on fluid dynamics in six-strand tundish: A numerical study

M. Mohammadi Soleymani ¹, K. Dolati Asl ², E. Mehrabi Gohari ^{*3}

¹ Assistant professor of mechanical engineering, Payame Noor University (PNU), P.O. Box. 19395-3697, Tehran, Iran

² PhD of mechanical engineering, University of Hormozgan, Bandar Abbas, Iran

³ Assistant professor of mechanical engineering, Payame Noor University (PNU), P.O. Box. 19395-3697, Tehran, Iran

Abstract

Tundish, as a continuous metallurgical operator, provides steel for continuous casting molds with optimum flow rates, constant temperatures, uniform chemical compositions, and low porosity. The cleanliness of the molten steel entering the mold is affected by the type of flow pattern and the performance of the tundish in flotation and removal of non-metallic impurities. In this paper, the fluid flow and heat transfer in a tundish in 2 cases, without an obstacle and with an obstacle, the turbo-stop, which is installed at its bottom and across the melt input, is simulated using the Ansys Fluent at melt heights of 0.5, 0.65, and 0.75 m. Results show that the formation of the second circulating flow inside the obstacle is the most important reason for the input melt velocity reduction. Increasing the melt height leads to a more uniform and less turbulent flow. Furthermore, increasing the melt height from 0.5 m to 0.75 m leads to a 3 % reduction in the average flow velocity. The highest heat transfer loss is from the top surface of the tundish and thus, the most temperature gradient exists at the top surface of the melt. The flow movement paths from the tundish input show that the melt flow velocity towards the sides of the tundish is increased with the melt height inside it. Furthermore, higher melt height causes the formation of higher stagnant melt volume inside the tundish, which negatively influences the inclusion of absorption by the slag.

Keywords: Continuous casting; Steel making; Tundish; Fluid dynamics; Numerical modeling; Ansys fluent.

1. Introduction

The melt in the ladle is distributed in casting lines using a distributor device called tundish, Fig. 1. The casting time period is mainly influenced by the melt height inside the tundish. According to the hydrostatic pressure of the melt, more melt exits from the outlet nozzles as the melt inside the tundish is increased [1].

In the steel continuous casting process, the

tundish provides sufficient melt for creating and maintaining a continuous flow to the mold even during ladle substitutions. The ladles are periodically filled and returned from the steel-making process. Furthermore, the tundish can act as a filter container by floating the inclusions as a slag layer. If solid impurity particles are allowed to remain in the product, then surface defects such as the porosity and expansion scab can be formed in the subsequent rolling processes or lead to the internal local stress concentration which can decrease the fatigue lifetime of the product. To produce high-quality products, the molten steel needs to be protected from interacting with the air by the slag coverage on the melt free-surface and use the ceramic-made nozzles between the containers. Otherwise, the oxygen of the air reacts with the steel which leads to the formation of detrimental oxide inclusions [2-4].

**Corresponding author*

Email: e.mehrabi@pnu.ac.ir

Address: Payame Noor University (PNU), P.O. Box. 19395-3697, Tehran, Iran

1. Assistant Professor

2. PhD

3. Assistant professor



Fig. 1. Tundish of the South Kave Steel (SKS) Company.

Various numerical and experimental studies have been conducted to investigate the flow in the tundish by researchers [5-7]. Most researchers in the experimental method simulate water at room temperature and at uniform temperature and steady-state flow. Mickey and Thomas [8] and Sousa Rocha, et al. [9] have done mathematical modeling to analyze the flow in a tundish with a specific geometry. They simulated the three-dimensional flow of molten steel and its temperature changes in tundish in both steady and unsteady states using the K- ϵ turbulence model. They used the Lagrangian tracking model to analyze particle motion. In this research, the residence time and density of the number of particles with different sizes have been investigated. In a study of a ten-strand tundish in the form of physical modeling, it was found that among the ten tundish outlets, the output that has the minimum residence time and the emergence of the detector is observed earlier has the worst performance in separating the inclusions. Also, the distribution of the number of inclusions between the strands is the same for each size of the inclusions and the descending order of the number of inclusions is based on the descending order of the average retention time between the strands [10]. Other research [11-14] Using mathematical and physical modeling, the effect of using flow control equipment on porosity separation has been investigated.

In other studies, a novel swirling flow generator (SFG) is intended to be installed around the inlet of the submerged entry nozzle (SEN) in the tundish to generate a swirling flow in the SEN by utilizing gravitational potential energy. The radial pressure gradient force causes inclusion particles to move toward the center. In the central area in the SEN, the collision rate between inclusion particles and bubbles increases significantly. Thus, bubble injection in swirling flow is beneficial to the removal of inclusion particles [15, 16]. The use of experiments and numerical simulations for flow behaviors of the tundish has been done by researchers. CFD modeling methods were employed in the studies. The obtained CFD results were compared with the results of laboratory tests (using a tundish water model) [17, 18].

The South Kave Steel (SKS) company, one of the largest steel-production companies in Iran, has a plan for removing the inclusion from the melt and producing clean steel. The tundish type of this company is com-

pletely different from those used in other steel-making factories in terms of the tundish geometry, dimensions and melt capacity, input melt place, and the number of outlet nozzles. Therefore, the tundish of this company in 2 cases, without an obstacle and with an obstacle, turbo-stop, is modeled and simulated in current research. This will be used as the first phase of a larger research program which will provide for a comprehensive study of the distribution of nonmetallic inclusions flowing through tundish steel.

2. Materials and research methods

In the discussion of modeling, different steps should be taken. In the initial stage, it is necessary to define a specific model for the geometry of the problem. This will be done by Solid Works software and the model with a different format will be saved for reading in Ansys Fluent computing software. Finally, by selecting the appropriate modules for modeling, the constructed model is called. Since the flow of fluid at the inlet and outlet areas is turbulent, in order to mathematically model such a system, it is necessary to apply a series of assumptions to simplify the system:

A: The free surface is considered smooth. Due to the presence of slag coating on the melt, in most cases, researchers have avoided wavy movements on the melt surface and considered the surface to be smooth.

B: Any trapping of air or gas when the melt stream enters is avoided.

C: Since the density of molten steel is a function of temperature, floating forces will be generated due to the temperature difference between different points of the fluid. The presence of these buoyancy forces affects the behavior of the fluid flow in the tundish, so it will be effective in removing and floating impurities. Therefore, heat transfer is another important consideration in tundish operations. Basically, temperature changes in tundish melt are caused by the discharge of melt at different temperatures from the pan to tundish, as well as heat loss through the walls (conductive heat transfer to the atmosphere) and through the slag coating (radiant heat transfer) [13].

2.1. Tundish geometry

The geometric characteristics of the six-strand tundish used in South Kave Steel (SKS) Company are shown in Fig. 2. The height of the melt inside the tundish is between 50 and 80 cm, but its application range, which is mostly used in steel-making, is 60 to 65 cm. The diameter of the outlet nozzles is 17 mm. For modeling the obstacle geometry at the tundish bottom (in case 2), the obstacle is supposed to be a cylinder with a height of 27 cm, an internal diameter of 23 cm, and a wall thickness of 2 cm.

2.2. The governing equations

Navier-Stokes equations are used to solve the fluid dynamics inside the tundish [19].

1) Continuity equation

$$\frac{\partial \rho}{\partial t} + \rho(\nabla u) = 0 \quad \text{Eq. (1)}$$

2) Momentum equation

$$\rho \frac{\partial u}{\partial t} + \rho[u \cdot \nabla]u = -\nabla P + \mu_{eff} \nabla^2 u + \rho g \quad \text{Eq. (2)}$$

Where t is time, ρ is the fluid density, u is velocity, p is pressure, g is the acceleration of gravity, and μ_{eff} is effective turbulent viscosity. Which is μ_{eff} the sum of μ molecular viscosity and μ_t turbulent viscosity.

$$\mu_{eff} = \mu + \mu_t = \mu + \rho C_\mu \frac{k^2}{\varepsilon} \quad \text{Eq. (3)}$$

and $C_\mu = 0.09$

3) Turbulence equations

Two standard equations are used to express the model k - ε in turbulence modeling, k which are two equations for the kinetic energy transfer of turbulence, and ε its displacement rate. The equation for turbulent kinetic energy is as follows.

$$\rho \frac{\partial k}{\partial t} + \rho \frac{\partial k u_i}{\partial x_i} = \frac{\partial}{\partial x_j} \left[\left(\mu + \frac{\mu_t}{\sigma_k} \right) \frac{\partial k}{\partial x_j} \right] + G_k - \rho \varepsilon \quad \text{Eq. (4)}$$

The G_k kinetic energy production of turbulence is from the mean velocity gradient and is obtained from Eq. 5.

$$G_k = \mu_t \frac{\partial u_j}{\partial x_i} \left(\frac{\partial u_i}{\partial x_j} + \frac{\partial u_j}{\partial x_i} \right) \quad \text{Eq. (5)}$$

The turbulent energy dissipation rate is obtained from Eq. 6.

$$\rho \frac{\partial \varepsilon}{\partial t} + \rho \frac{\partial \varepsilon u_i}{\partial x_i} = \frac{\partial}{\partial x_j} \left[\left(\mu + \frac{\mu_t}{\sigma_\varepsilon} \right) \frac{\partial \varepsilon}{\partial x_j} \right] + C_{1\varepsilon} \frac{\varepsilon}{k} G_k - C_{2\varepsilon} \rho \frac{\varepsilon^2}{k} \quad \text{Eq. (6)}$$

That x_i and x_j are the Cartesian components of velocity and the experimental turbulence constants are shown in Table 1.

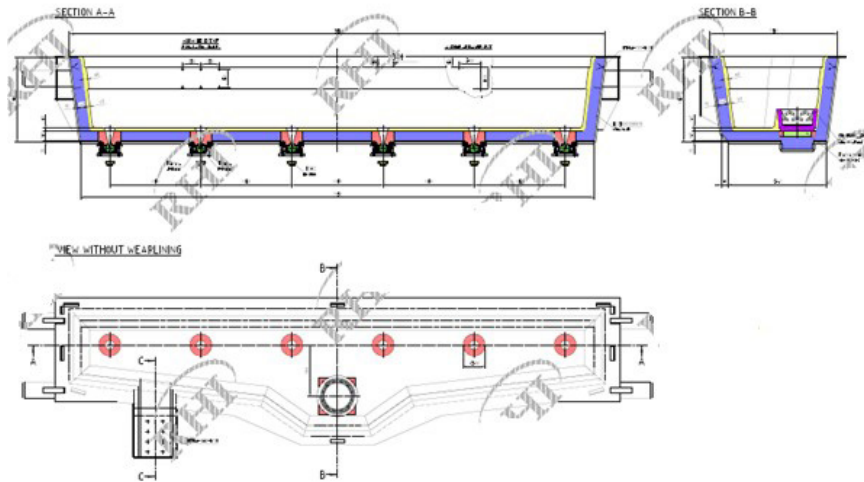


Fig. 2. Tundish geometric characteristics.

Table 1. The proposed experimental constants of turbulence [19].

$C_{1\varepsilon}$	$C_{2\varepsilon}$	σ_k	σ_ε	C_μ
1.38	1.92	1	1.3	0.09

4) Energy equation

An energy equation is needed to calculate the temperature of the molten fluid.

$$\frac{\partial}{\partial t}(\rho E) + \nabla \cdot [u(\rho E + P)] = \nabla \cdot \left(k_{eff} \nabla T - \left(h + \frac{P}{\rho} \right) + (\tau_{eff} \cdot u) \right) \quad \text{Eq. (7)}$$

That T is temperature and τ_{eff} is the viscous dissipation term and k_{eff} is effective conductivity and from the relation $k_{eff} = k + k_t$ it follows that k_t is the turbulent thermal conductivity. The energy E is obtained from Eq. 8. Also, h is reference temperature and C_p is constant pressure heat capacity.

$$E = h - \frac{P}{\rho} + \frac{u^2}{2} \quad \text{Eq. (8)}$$

Also, $h = \int_{T_{ref}}^T C_p dT$ is and T_{ref} is reference temperature and C_p is constant pressure heat capacity.

2.3. Thermal properties and boundary conditions

The mass flow rate of the inlet melt to the tundish

is 50 kg s^{-1} and its temperature is 1530°C , which is close to the actual conditions. Melt density is a function of temperature and is equal to $\rho = 7010 - 0.883(T - 1818)$. The viscosity is $0.007 \text{ kg m}^{-1} \text{ s}^{-1}$ and the heat capacity is $720 \text{ J kg}^{-1} \text{ K}^{-1}$ and the thermal conductivity is $33 \text{ W m}^{-1} \text{ K}^{-1}$. Because the walls of the melt and the top surface of the melt exchange heat with the surrounding environment, and because the temperature of the melt and the melt is higher than the ambient temperature, heat is transferred from the melt to the environment and the melt temperature decreases. Based on previous studies [19, 20], the amount of heat loss from the top surface of the melt, hard floor, and hard walls are $15, 1.5,$ and 3.5 kW/m^2 , respectively (Table 2).

Because of the symmetry in the overall geometry of the tundish, only half of the tundish is considered the computational domain, which according to Fig. 3, one side of the domain is defined by the symmetry boundary condition. The side walls and the floor of the ramp are marked with the condition of non-slip. The upper level of the solution amplitude is empty space, which is why the condition without shear stress is used. The melt flow inlet at the top of the slope is considered the velocity input and the melt flow output at the bottom of the geometry is considered the pressure output (pressure equal to atmospheric pressure).

Table 2. Thermal properties of the melt and boundary conditions of heat dissipation [19].

Thermal properties		heat transfer loss	
melt density	$\rho = 7010 - 0.883(T - 1818)$	melt top surface	15 kW m^{-2}
melt viscosity	$0.007 \text{ kgm}^{-1}\text{s}^{-1}$	tundish bottom	1.5 kW m^{-2}
thermal capacity	$720 \text{ J kg}^{-1}\text{K}^{-1}$	tundish walls	3.5 kW m^{-2}
thermal conduction coefficient	$33 \text{ W m}^{-1}\text{K}^{-1}$		

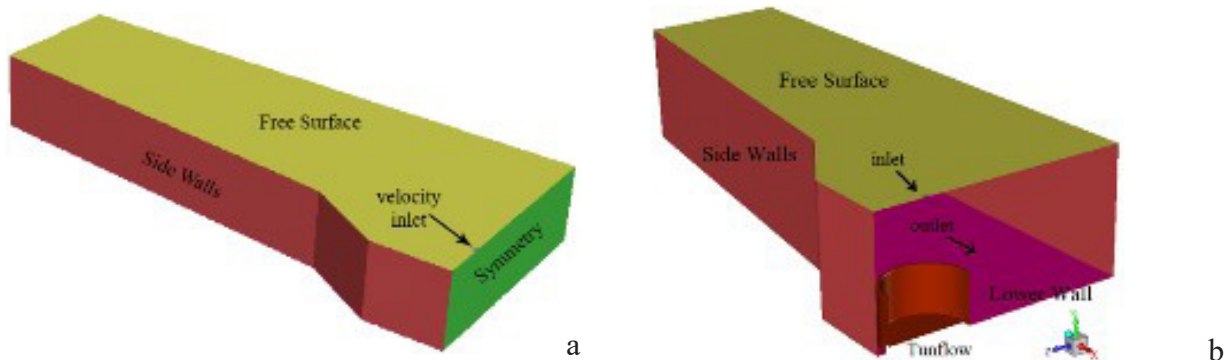


Fig. 3. Model of solution domain created in Ansys software a) without an obstacle b) with an obstacle.

Since the height of the melted fluid inside the tundish is variable, in the present study, the amount of melt height inside the tundish is considered in three states of 50, 65, and 75 cm, based on which three solution amplitudes are modeled. In the present study, the variable h indicates the amount of melt height within the tundish. The meshes used for each case (different heights) ranged from 3.3 to 3.7 million grids. At the same time, the sensitivity analysis for the suitable mesh has also been done. A model similar to reference [19] was run in Ansys Fluent and the results were consistent. The temperature at different points of the Tundish and the exit speed of the nozzle in industrial trials were calculated and the results were consistent with the modeling of this research.

3. Results and discussion

In this study, the tundish behavior of the flow pattern and heat distribution in 2 cases, without an obstacle and with an obstacle, turbo-stop, was investigated. Figs 4 and 5 show part of the movement path of the input melt to the tundish at two melt heights of $h = 0.5\text{m}$ and $h = 0.75\text{m}$ without an obstacle and with obstacle case. As observed,

the input melt flow to the tundish impacts the bottom surface (or obstacle bottom surface) inside the tundish vertically and uniformly due to the high velocity of the input flow. After impacting the obstacle walls, the flow moves upward and then the fluid flow circulation inside the tundish is started. The highest fluid flow velocity and turbulence occur in the middle part of the tundish which is nearer the input melt flow region. At the end of the tundish, the existent melt is less affected by the tundish input. A comparison between Figs. 4 and 5 shows that the movement and turbulence of the molten fluid flow are increased at the middle and end part of the tundish respectively, by decreasing and increasing the melt height inside the tundish. Furthermore, it can be inferred from the comparison that the direct input fluid flow effect and mixing and turbulence in the flow are reduced as the melt height is increased. Therefore, to have a more laminar flow that enhances the movement of inclusion towards the free surface of the fluid, the melt height is better to be increased. Besides, according to Figs. 4 and 5, the reflected flow from the nearer wall to the input melt region moves to a higher height. Therefore, reducing the intensity of this flow would be a proper way for decreasing the turbulence in the inclusion.

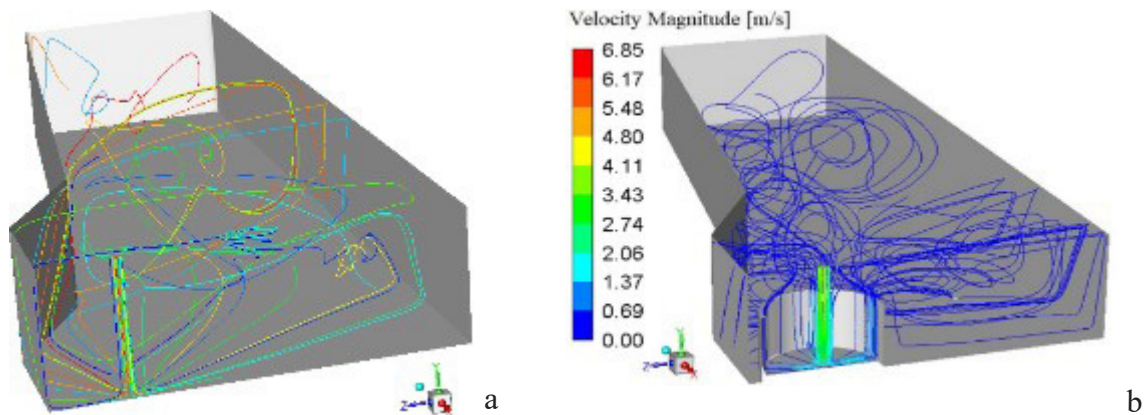


Fig. 4. Part of the path of the incoming melt to Tundish ($h = 0.5\text{m}$)
 a) without an obstacle b) with an obstacle.

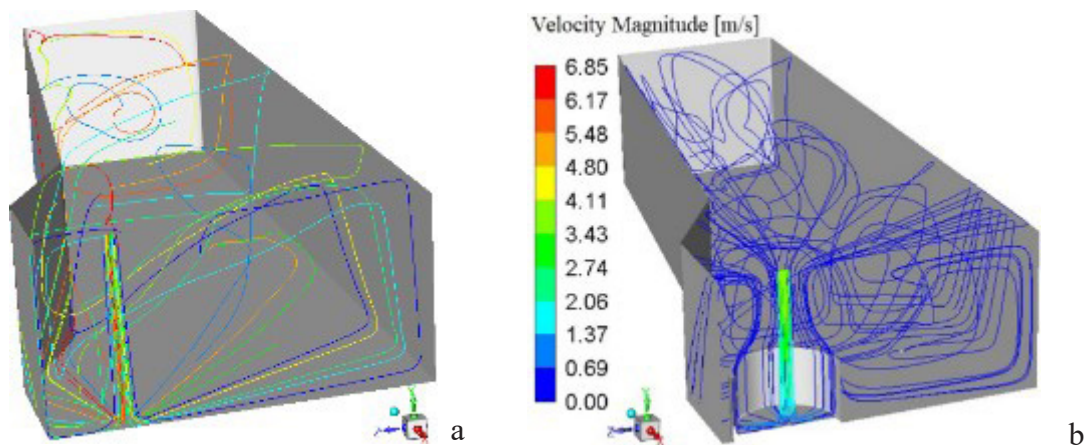


Fig. 5. Part of the inlet melt path to the tundish ($h = 0.75\text{m}$)
 a) without an obstacle b) with an obstacle.

The obstacle at the tundish bottom (in the case of an obstacle) is installed for controlling the entering melt into the tundish, and the flow paths are shown in Fig. 6 in a magnified view. The input flow moves towards the tundish bottom with high velocity and after impacting the obstacle bottom moves upwards due to the obstacle walls. As observed, part of the reflected upward-moving flow is driven towards the input flow due to the pressure reduction near that. Therefore, a secondary circulating flow is formed inside the obstacle. Part of the obstacle which is nearer to the tundish wall has the lowest circulating flow.

Fig. 7 shows the melt velocity vector on a longitudinal plane passing through the outputs (in the case without an obstacle). It should be noted that for a better display of velocity vectors in low-velocity areas, the maximum velocity is 0.2 m/s. The melt jet strikes the impact pad hard on the floor of the tundish and the melt expands radially. In the upper part of tundish, you can see areas

with above-average speed as well as an area with very low speed. When the upstream flow from the inlet to the farthest sides of the tundish, it returns from the bottom to the inlet area at above-average velocities. This produces some shock due to the downstream current. Based on Fig. 7, it can be clearly seen that there is less melt flow in places far from the center of the tundish.

The flow path in the symmetry plane of the tundish in the case of an obstacle is shown in Fig. 8. The maximum fluid flow velocity is related to the input flow and flows on the internal walls of the obstacle. As mentioned before, the secondary circulating flow inside the obstacle is harsh, which has a considerable effect on the flow velocity reduction in the tundish. According to Fig. 8, the melt flow exists in all points of the symmetry plane, but the velocity is different at different points of the plane. Finally, a more regular flow can have certain advantages for the quality of the steel, such as better thermal homogenization and greater particle removal.

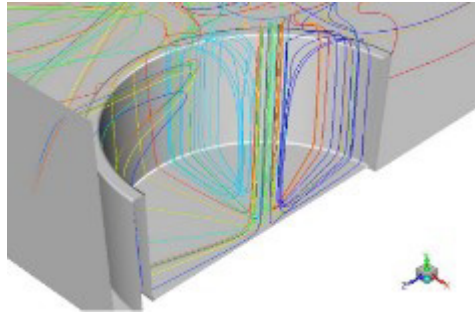


Fig. 6. The obstacle at the tundish bottom (in the case of an obstacle), which is installed for controlling the entering melt into the tundish, and the flow paths.

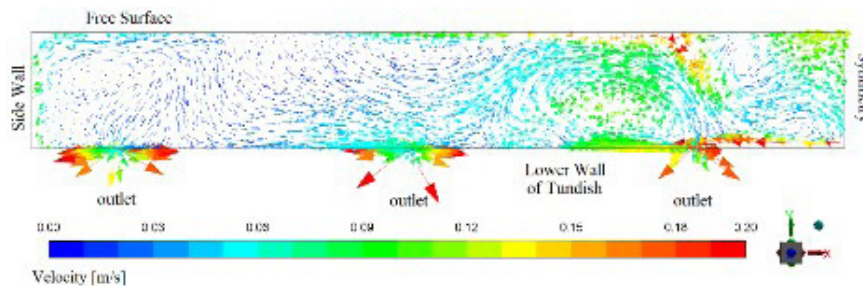


Fig. 7. The melt velocity vector on a longitudinal plane passing through the outputs (in the case without an obstacle).

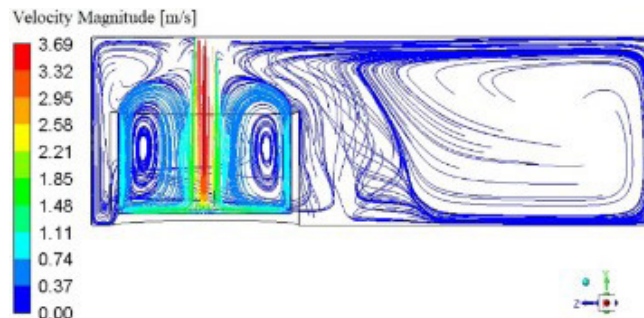


Fig. 8. The flow path at the symmetry plane of the tundish in the case with an obstacle $h=0.5\text{m}$.

The velocity contours in the symmetry plane of the tundish in the case of obstacle are shown in Fig. 9 and Fig. 10 for $h = 0.5$ m and $h = 0.75$ m, respectively. The highest flow velocity belongs to the input flow to the tundish, which its velocity is remarkably reduced after impacting the obstacle. The input flow has to move a longer path as the melt height is increased and because the density and viscosity of the melt are high, the input flow velocity is reduced remarkably. Therefore, the impact velocity of the flow onto the obstacle is decreased with the melt height. Furthermore, it can be concluded by comparing Figs. 9 and 10 that the circulating flow intensity and flow turbulence are considerably decreased as the melt height inside the tundish is increased, which has a considerable effect on the inclusion formation as well.

The overall absolute velocity contours on the melt top and side surfaces in 2 cases, without an obstacle, and with an obstacle, turbo-stop, are shown in Figs 11 to

13 for melt heights of 0.5, 0.65, and 0.75 m. The maximum flow velocity is 0.73 m/s occurring at the melt input to the tundish, for all three melt heights. For a better contour representation, the maximum velocity is set to 0.5 m/s to better observe the velocity changes. Since the no-slip boundary condition is applied to the sidewalls of the tundish, the flow velocity is zero there. As observed, the maximum flow velocity on the melt surface is not changed considerably with the melt height and is nearly by the input melt to the tundish. The average velocity on the melt surface is calculated to be 0.0765, 0.0753, and 0.0745 m/s for $h = 0.5$, 0.65, and 0.75 m, respectively. Therefore, the average velocity also does not change considerably with the melt height. However, the absolute flow velocity is changed more uniformly near the melt input as the melt height is increased. Furthermore, the tundish with a higher melt height has more still regions. Higher still melt volume in the tundish has a negative effect on the inclusion absorption ⁴⁾.

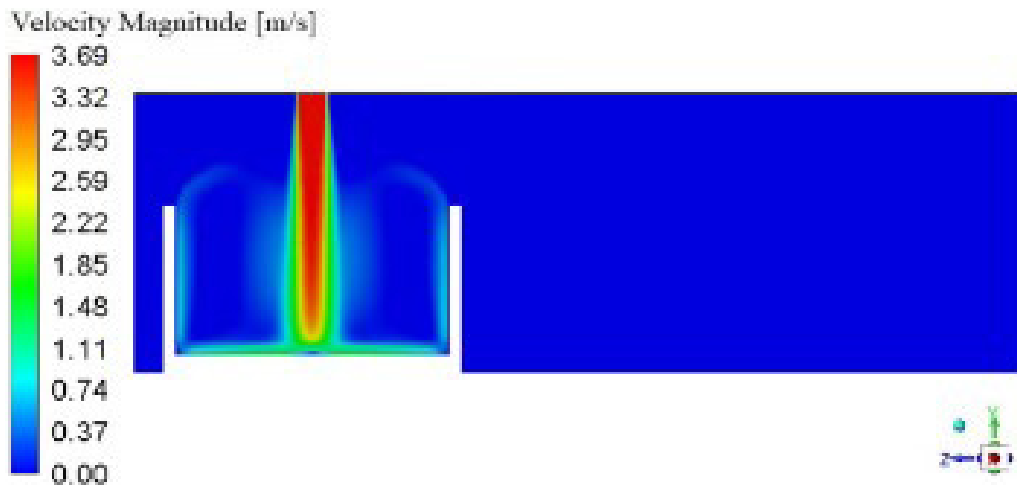


Fig. 9. The velocity contours in the symmetry plane of the tundish in the case of obstacle $h=0.5$ m.

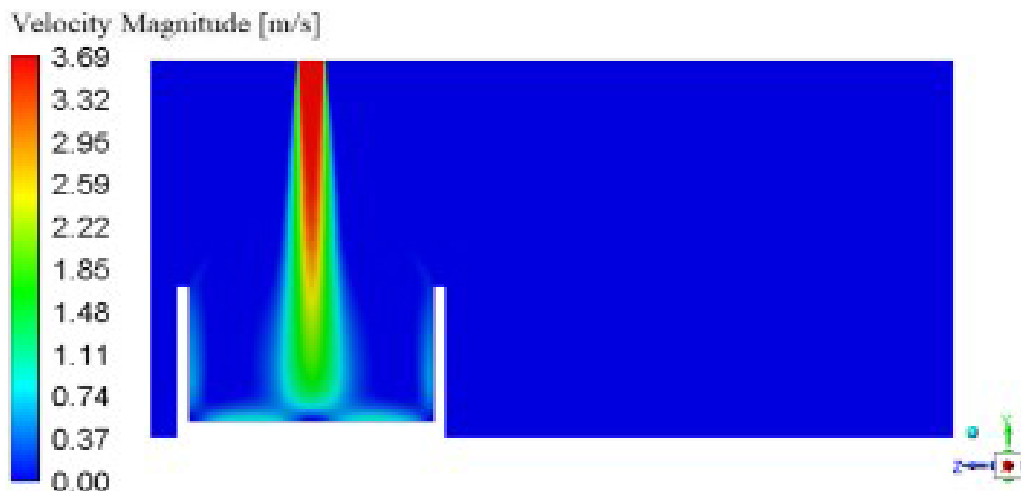
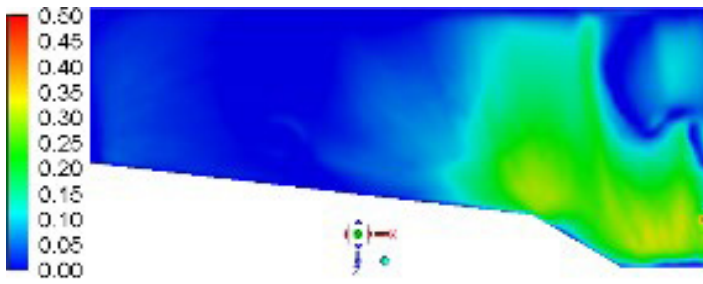
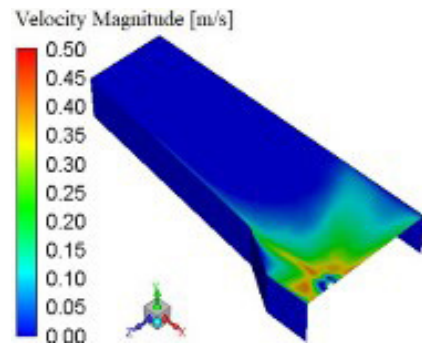


Fig. 10. The velocity contours in the symmetry plane of the tundish in the case of obstacle $h=0.75$ m.

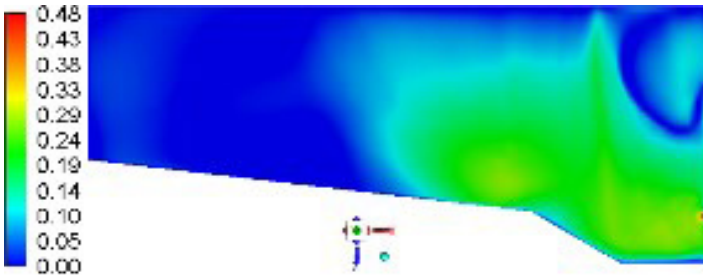


a

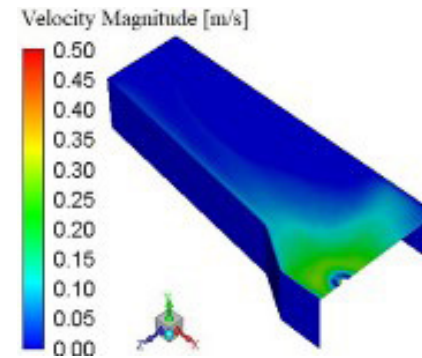


b

Fig. 11. The overall absolute velocity contours on the melted top and side surfaces $h=0.5\text{m}$
a) without an obstacle b) with an obstacle.

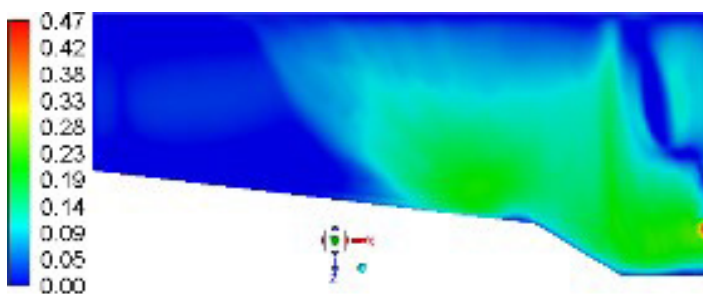


a

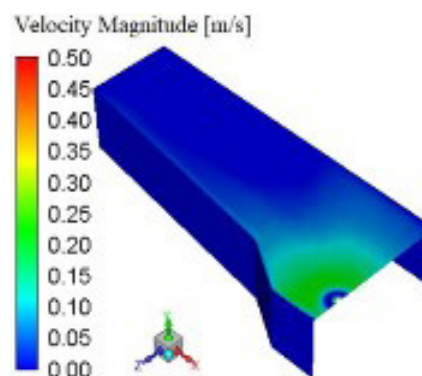


b

Fig. 12. The overall absolute velocity contours on the melted top and side surfaces $h=0.65\text{m}$
a) without an obstacle b) with an obstacle.



a



b

Fig. 13. The overall absolute velocity contours on the melted top and side surfaces $h=0.75\text{m}$
a) without an obstacle b) with an obstacle.

Fig. 14 shows the velocity vectors on a longitudinal surface passing the outlets for $h=0.5$ and 0.75m (in the case of an obstacle). It should be mentioned that the maximum velocity is considered to be 0.12 m/s for a better representation of the velocity vectors in low-velocity regions. In both conditions, the circulating flow regions are clearly observed with a higher intensity at $h=0.5\text{m}$, which influences the slag. As the melt height is increased, the outlet flow velocity is increased, leading to faster casting.

Figs 15 and 16 show the absolute temperature and velocity counters on the lateral walls of the tundish and the upper surface of the melt (in the case without an obstacle), which cause heat loss to the environment, respec-

tively. For a better display of fluid velocity counters, the maximum velocity value in this contour is 0.45 m/s . In these two Figs, a very good correlation is observed between fluid dynamics and temperature distribution; as the melt moves faster, it loses more heat due to an increase in the amount of heat transfer coefficient. The difference between the inlet temperature (1530°C) and the coldest tundish point (1518°C) is only 12°C . One of the ways to make the outlet flow of the tundish more uniform is to make the melt in the tundish more uniform in terms of heat. Accordingly, the use of turbo stops (obstacles) to melt movement in the tundish is recommended to make the melt flow more uniform.

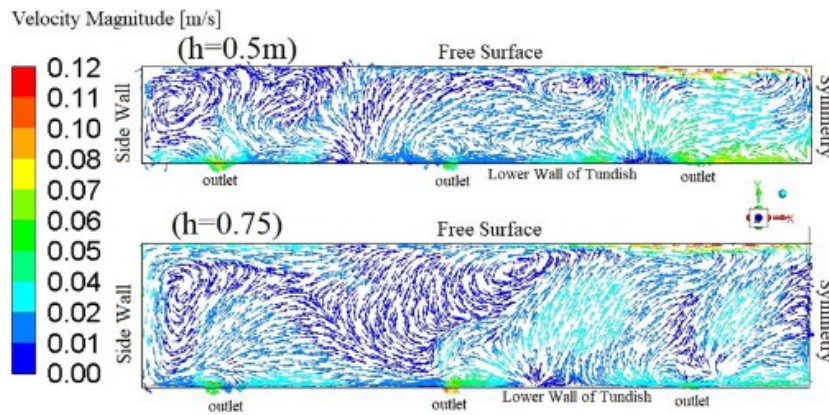


Fig. 14. The velocity vectors on a longitudinal surface passing the outlets for $h=0.5\text{m}$ and 0.75m (in the case of an obstacle).

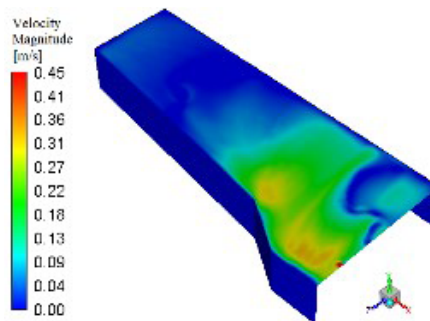


Fig. 15. The absolute velocity counters on the lateral walls of the tundish and the upper surface of the melt $h=0.5\text{m}$ (in the case without an obstacle).

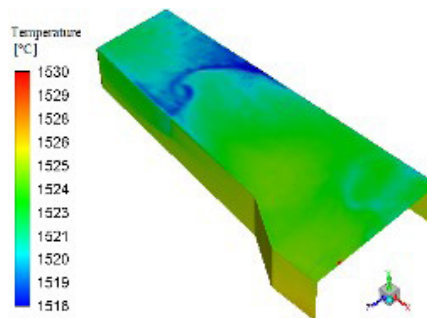


Fig. 16. The absolute temperature counters on the lateral walls of the tundish and the upper surface of the melt $h=0.5\text{m}$ (in the case without an obstacle).

The melt temperature contours on the top and side surfaces of the tundish in the case of an obstacle are shown in Fig. 17 and Fig. 18, respectively. The average temperature on top and side surfaces is 1524.2°C and 1524°C respectively for $h=0.5\text{m}$ and $h=0.75\text{m}$, which is almost the same value. However, surfaces with the maximum temperature, at the top surface of the melt, are reduced with the melt height. Since the density of the molten steel is varied with the temperature, the buoyancy forces are formed in the tundish due to the temperature difference in the melt. The presence of the buoyancy forces changes the flow behavior such that the inclusion removal and floating are influenced by them. Therefore, the heat transfer in the tundish is another important factor that needs to be considered. The temperature changes of the melt are due to pouring melt with different temperatures from the ladle and heat losses from the tundish walls, through the conduction, and the slag coverage through the radiation.

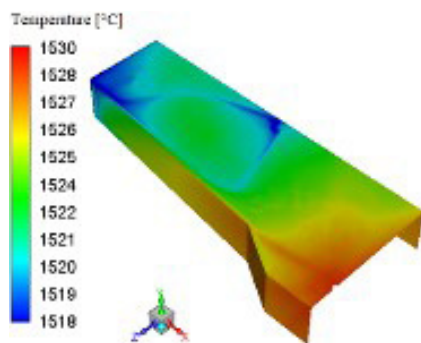


Fig. 17. The melt temperature contours on the top and side surfaces of the tundish in the case of an obstacle $h=0.5\text{m}$.

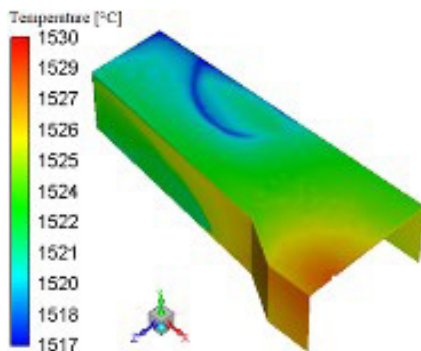


Fig. 18. The melt temperature contours on the top and side surfaces of the tundish in the case of an obstacle $h=0.75\text{m}$.

4. Conclusions

The following results are obtained from modeling and simulation of the steel continuous casting tundish for evaluating and comparing the flow pattern:

- The use of turbo stops to melt movement in the tundish makes the melt flow more uniform, and a more regu-

lar flow can have certain advantages for the quality of the steel, such as better thermal homogenization and greater particle removal.

- A strong circulating flow is formed inside the tundish because the input melt flow directly enters the obstacle center.
- The molten fluid flow turbulence is reduced by increasing the melt height in the tundish.
- Analysis of the input flow into the tundish indicates that the input flow has a maximum and minimum effect on the middle and side regions of the tundish, respectively.
- The average flow velocity on the top surface of the melt is decreased by %3 by increasing the melt height from 0.5 to 0.75 meters.
- Since the heat transfer and loss are highly dependent on the velocity of the molten fluid flow, increasing the melt height leads to a more laminar fluid flow inside the tundish and thus the heat loss and temperature gradient inside the tundish are reduced.
- Tundish with a higher melt height has more static melt areas which negatively influence the amount of particle absorption.

Acknowledgments

This research was accomplished with the support of SKS. Special thanks to the generous help of R&D and the steel-making unit of SKS; the authors would like to gratefully appreciate H. Soltani, T. Adhami, and S. Lak for their help in this study.

Reference

- [1] S. Louhenkilpi, Continuous casting of steel, Elsevier, 2014. <https://doi.org/10.1016/B978-0-08-096988-6.00007-9>.
- [2] S. Yang, L. Zhang, J. Li, K. Structure optimization of horizontal continuous casting tundishes using mathematical modeling and water modeling. *ISIJ international*. 49 (2009) 1551-1560. <https://doi.org/10.2355/isijinternational.49.155>.
- [3] X. Zhou, Z. Tang, G. Qu, Thermal stress and thermal fatigue analysis of the continuous casting tundish cover. *Materials Science and Engineering: A*. 527 (2010) 2327-2334. <https://doi.org/10.1016/j.msea.2009.11.068>.
- [4] Z. Li, M. Zhang, F. Zhou, Y. Lu, X. Zhang, H. Gu, 2022. Numerical simulation of slag entrapment process during the end of casting in tundish, *Ironmaking & Steelmaking*. (2022) 1-9. <https://doi.org/10.1080/03019233.2022.2078261>.
- [5] M.R. Mosalman Yazdi, A.R. Faghieh Khorasani, S. Talebi, Physical modeling of melt flow in steel continuous casting tundish, *Modares Mechanical Engineering*. 17 (2017) 385-392 (in Persian). <https://dorl.net/dor/20.1001.1.10275940.1396.17.6.25.5>.
- [6] J.G. Liu, H.C. Yan, L.I.U. Liu, X.H. Wang, Water

- modeling of optimizing tundish flow field, *Journal of iron and steel research International*. 14 (2007) 13-19. [https://doi.org/10.1016/S1006-706X\(07\)60036-3](https://doi.org/10.1016/S1006-706X(07)60036-3).
- [7] A. Kumar, D. Mazumdar, S.C. Koria, Modeling of fluid flow and residence time distribution in a four-strand tundish for enhancing inclusion removal, *ISIJ international*. 48 (2008) 38-47. <https://doi.org/10.2355/isijinternational.48.38>.
- [8] Y. Miki, B.G. Thomas, Modeling of inclusion removal in a tundish, *Metallurgical and materials transactions B*. 30 (1999) 639-654. <https://doi.org/10.1007/s11663-999-0025-6>.
- [9] J.R. de Sousa Rocha, E.E.B. de Souza, F. Marcondes, J.A. de Castro, Modeling and computational simulation of fluid flow, heat transfer and inclusions trajectories in a tundish of a steel continuous casting machine, *Journal of Materials Research and Technology*. 8 (2019) 4209-4220. <https://doi.org/10.1016/j.jmrt.2019.07.029>.
- [10] S.G. Zheng, M.Y. Zhu, Y.L. Zhou, W. Su, Flow characteristics and inclusion removal in a ten-strand continuous casting tundish: Physical Modelling and Industrial Trials, *Journal of Iron and Steel Research International*. 23 (2016) 92-97. [https://doi.org/10.1016/S1006-706X\(16\)30018-8](https://doi.org/10.1016/S1006-706X(16)30018-8).
- [11] L. Zhang, S. Taniguchi, K. Cai, Fluid flow and inclusion removal in continuous casting tundish, *Metallurgical and Materials Transactions B*. 31 (2000) 253-266. <https://doi.org/10.1007/s11663-000-0044-9>.
- [12] P.K. Jha, P.S. Rao, A. Dewan, Effect of height and position of dams on inclusion removal in a six strand tundish, *ISIJ international*. 48 (2008) 154-160. <https://doi.org/10.2355/isijinternational.48.154>.
- [13] C.M. Fan, R.J. Shie, W.S. Hwang, Studies by mathematical and physical modelling of fluid flow and inclusion removal phenomena in slab tundish for casting stainless steel using various flow control device designs, *Ironmaking & Steelmaking*. 30 (2003) 341-347. <https://doi.org/10.1179/030192303225004015>.
- [14] H.H. Zhu, M. Wang, C. Yao, Z.L. Wang, X.L. Wang, Y.P. Bao, Influence of non-iso-velocity casting on flow-field index of a 41-ton six-strand tundish by physical and numerical modeling, *Journal of Iron and Steel Research International*. (2022) 1-13. <https://doi.org/10.1007/s42243-022-00821-4>.
- [15] Z.Y. Xin, H.N. Cui, T. Li, G.Z. Tang, Y.L. Zhu, J.C. Yan, J.G. Li, Numerical Simulation of Inclusion Removal by Bubble Injection in the Submerged Nozzle With Swirling Flow, *Metallurgical and Materials Transactions B*. (2022) 1-17. <https://doi.org/10.1007/s11663-022-02552-z>.
- [16] J. Lu, S. Li, Z. Luo, Z. Zou, L. Shao, Numerical simulation of collision removal of inclusion in swirling flow tundish, *International Journal of Chemical Reactor Engineering*. (2022). <https://doi.org/10.1515/ijcre-2021-0300>.
- [17] T. Merder, J. Pieprzyc, M. Warzecha, P. Warzecha, A. Hutny, Evolution of the Numerical Model Describing the Distribution of Non-Metallic Inclusions in the Tundish, *Materials*. 14 (2021) 2229. <https://doi.org/10.3390/ma14092229>.
- [18] J. Liu, P. Zhou, X. Zuo, D. Wu, D. Wu, Optimization of the Liquid Steel Flow Behavior in the Tundish through Water Model Experiment, Numerical Simulation and Industrial Trial, *Metals*. 12 (2022) 1480. <https://doi.org/10.3390/met12091480>.
- [19] O.S. Delgado Ramirez, E. Torres-Alonso, J.Á. Ramos Banderas, S.A. Arreola Villa, C.A. Hernández Bocanegra, J.S. Téllez Martínez, Thermal and Fluid-Dynamic Optimization of a Five Strand Asymmetric Delta Shaped Billet Caster Tundish, *Steel research international*. 89 (2018) 1700428. <https://doi.org/10.1002/srin.201700428>.
- [20] O. Minin, I. Minin, *Computational Fluid Dynamics Technologies and Applications*. BoD—Books on Demand, 2011. <https://doi.org/10.5772/686>.